Theor Chem Acc (2010) 127:293–302
DOI 10.1007/s00214-009-0715-9

REGULAR ARTICLE

An amber compatible molecular mechanics force field for the anticancer drug topotecan

Giovanni Chillemi · Andrea Coletta · Giordano Mancini · Nico Sanna · Alessandro Desideri

Received: 22 July 2009 / Accepted: 2 December 2009 / Published online: 19 December 2009

Abstract A molecular mechanics (MM) force field has been developed for the topotecan (TPT) molecule, an anticancer drug the only molecular target of which is the human topoisomerase I-DNA covalent complex. We proceeded according to the *amber03* force field parametrization protocol, based on quantum mechanical calculations with solvent effects included by means of continuum models. An adequate description of the electronic states of TPT has been ensured comparing calculated IR vibrational frequencies and NMR chemical shifts with experimental results. Bonded molecular parameters have been verified by comparison with ab initio normal mode vibrational analysis, while atomic charges have been fitted either using the restrained electrostatic potential fitting (RESP) or the multi-conformational RESP (MultiRESP) procedures. Particular attention has been paid to the parametrization of the dimethylamino group in ring A, for which several energy minima were found. The reliability of the force field has been checked comparing the results obtained from a classical molecular dynamics simulation with quantum mechanics ab initio energy calculations. The development of the topotecan force field makes it possible to carry out reliable simulations of the topotecan–topoisomerase–DNA ternary complex, thus allowing the investigation of important biological questions, such as the selective resistance to topotecan caused by single residue topoisomerase I mutations.

Keywords Force field · Molecular dynamics · Anticancer · Camptothecin · Topotecan · Topoisomerase · Amber · Molecular mechanics · Gromacs · Metadynamics

1 Introduction

Camptothecin (CPT), is a naturally occurring alkaloid extracted from the Chinese tree *Camptotheca acuminata* [1], from which a class of antitumoral agents has been derived. For example, topotecan (Hycamtin, GlaxoSmithKline) is a widely used agent to treat lung and ovarian carcinoma while irinotecan (Camptofar, Pfizer) is used to treat colorectal cancer. Several other CPT derivatives are currently under development [2]. The anticancer activity of CPTs is due to the inhibition of topoisomerase I (Top1): an ubiquitous class of enzymes essential for the control of DNA supercoiling generated by replication, transcription, and recombination [3]. Analysis of X-ray structures of Top1 and DNA in complex with CPT (or CPT derivatives) has provided a nanoscopic level explanation on topoisomerase inhibition and of Top1 resistance to CPTs caused by single point mutations near the binding site [4–6]. However, several other mutations (such as Ala653Pro, Glu418Lys, and Thr729Lys [7–10] exist that make Top1 resistant to CPT but are located far from the active site; in such cases simple inspection of ternary complex crystals cannot alone explain the resistance to CPT of these mutants. A further hint of the importance of

Electronic supplementary material The online version of this article (doi:10.1007/s00214-009-0715-9) contains supplementary material, which is available to authorized users.

G. Chillemi (✉) · G. Mancini · N. Sanna
CASPUR Interuniversities Consortium for Supercomputing Applications, Via dei Tizii 6b, 00185 Rome, Italy
e-mail: g.chillemi@caspur.it

A. Coletta · A. Desideri
Department of Biology, University of Rome Tor Vergata, Via Della Ricerca Scientifica, 00133 Rome, Italy

long-range communications is the existence of other mutations, such as Lys681Ala or Thr718Ala, which have an effect analogous to that of CPT on the enzyme [11, 12]. A first MD study on the Top1–DNA–CPTs ternary complexes, focused on the free energy barriers for drug dissociation, has recently been reported [13], while binding of TPT with a nicked DNA has been investigated by computational and NMR data [14], demonstrating the utility of an adequate computational model to rationalize experimental data. Novel computational approaches, based on state-of-the-art quantum–mechanical (QM) calculations, have already been demonstrated to adequately describe the structural and electronic properties of TPT and CPT and reproduce UV–Vis spectroscopic observations [15, 16]. This electronic and molecular characterization of the anticancer drugs in aqueous solvent allows the building of an accurate force field to be used in molecular dynamics (MD) study of the Top1–DNA–drug ternary complex that may explain the structural long-range effects observed in some resistant Top1 mutants.

In this work we describe the parametrization of a classical molecular mechanics (MM) force field, capable of reproducing internal flexibility and intermolecular interactions of the CPT derivative topotecan. Several structures of TPT are stable at different pH values, differing for the E ring state (in the lactonic or carboxylate form) and for the protonation state of the side chain groups on ring A. In a previous work we have defined as type 1a and 1b the two possible lactonic forms stable around pH 5 (see Fig. 1 in [15]); as type 2a and 2b the two possible lactonic forms stable around neutral pH (see Fig. 2 in [15]; as type 3a and 3b the two possible carboxylate forms also stable around neutral pH (see Fig. 4 in [15]). For coherence, we will maintain this naming scheme here. Both type 2 and type 3 forms are compatible with existing crystallographic structures of the Top1–DNA–TPT ternary complex [5]. Since the lactonic form is considered the active one [17], we focused this study on the force field parametrization of the two tautomers of the lactonic forms: i.e. type 2a and 2b (Fig. 1).

2 Methods

The electronic state for the type 2a and 2b TPT forms was characterized by quantum mechanical (QM) calculations with the Gaussian03 package [18], by properly tuning the level of accuracy of the adopted methods. In particular, geometry optimization of the different conformations of TPT have been performed at HF/3-21G level of theory, followed by further refinement at B3LYP/6-31G*. In all calculations, solvent effects have been included by means of the COSMO variant of the polarizable continuum model (PCM) [19]. PCM(B3LYP/6-31G*) ab initio frequencies were scaled by the factor 0.9613, as carried out by other authors [20–22], since it is known that the ab initio normal modes overestimate the experimental values. Classical normal modes were calculated with the *nmodes* program [23]. Theoretical chemical shift (in ppm with respect to tetramethylsilane, TMS) has been derived from magnetic shielding calculated with the gauge independent atomic orbital method (GIAO) [24] using the formula:

$$\delta_i = \sigma_{\mathrm{TMS}} - \sigma_i$$

where δ_i is the ^{13}C chemical shift of the i-th atom σ_i its magnetic shielding, and $\sigma_{\mathrm{TMS}} = 188.1$ [25], the magnetic shielding of our reference.

Starting from the QM results, we developed a force field to be used in simulations of Top1–DNA–TPT complexes in aqueous solution. Molecular mechanics intra-molecular parameters were obtained using the *antechamber* software in the AMBER suite, generating a set of parameters compatible with the Amber 2003 (*amber03*) force field [26]. Then, atomic charges were fitted with the RESP method

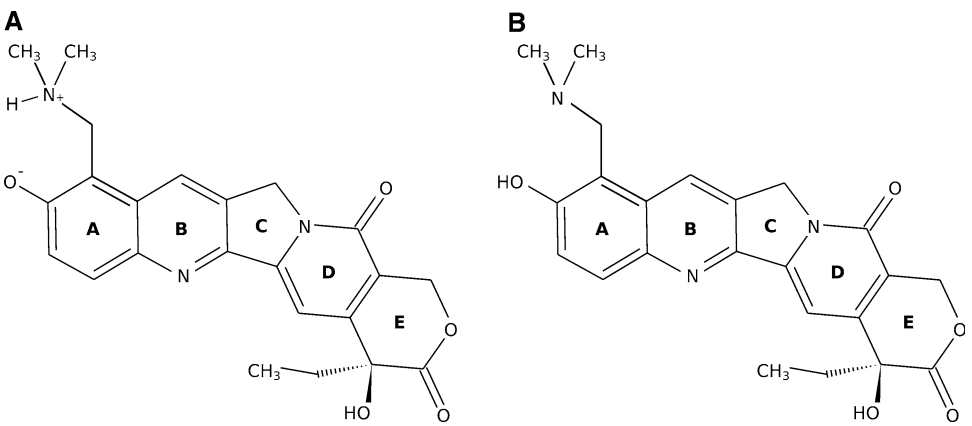

Fig. 1 Schematic representation of the lactonic tautomers of TPT present under physiological conditions. Substituent groups on ring A are specific of topotecan as compared to camptothecin. **a** Type 2a with protonated nitrogen of the dimethylamino group; **b** type 2b with neutral dimethylamino group

[27, 28]. Subsequently, only for the type 2b structure, the atomic charges have been calculated applying the multi-conformation RESP (MultiRESP) procedure [29], which takes into account more than one conformation of minimum energy via the following equation:

$$C(n) = \frac{\sum_i C_i(n) e^{\frac{-\Delta E_i}{kT}}}{\sum e^{\frac{-\Delta E_i}{kT}}} \quad (1)$$

where $C(n)$ is the MultiRESP charge of the atom n; $C_i(n)$ is the charge of atom n in the conformation i; ΔE_i is the energy difference between the conformation i and the global minimum; k is the Boltzmann constant; T is the temperature (300 K in our case).

The AMBER topology was converted in GROMACS format using the amb2gmx.pl script [30], distributed with ffAMBER, the AMBER force field porting in the GROMACS molecular dynamics suite [31]. Classical MD simulations have been performed with the GROMACS-3.3.3 software. A single TPT molecule has been solvated in a box of dimensions $3.92 \times 3.16 \times 2.88$ nm^3 containing 1151 TIP3P water molecules. Simulations have been performed at constant temperature of 300 K by means of the Berendsen method [32] with a coupling constant of 0.1 ps. Electrostatic interactions were taken into account by means of the Particle Mesh Ewald method [33], using a cutoff radius of 1.2 nm in real space. A cutoff radius of 1.2 nm was chosen also for the van der Waals interactions. The linear constraint solver (LINCS) algorithm has been applied to constrain fast atomic motions [34]. Metadynamics simulations, using the same set of parameters of the other MD simulations, have been performed with GROMETA-3.3.3 package which implements the Parrinello–Laio biased potential technique [35]. Rotations about the dimethylamino group of ring A were used as meta-coordinates via the TORSION keyword and the potential wells were filled using Gaussian hills 0.5 kJ/mol high and 0.25 radians wide, deposed every 100 simulation steps. Other analyses have been carried out using GROMACS tools and in-house written codes. Dihedral autocorrelation functions were calculated $C(t) = \langle \cos[\theta(\tau) - \theta(t+\tau)] \rangle_T$ [36] and the time constant τ was estimated using the approximation expression for $C(t)$ proposed in the same paper: $C(t) = S_D^2 + (1 - S_D^2)e^{-t/r}$. Figure 11 was created using the CHIMERA package [37]; graphs were obtained with the Grace program [38] and PES plots have been produced with Octave [39] and Matplotlib [40] scripts. All the molecular mechanics parameters for the type 2a and 2b TPT forms are reported in the supplementary material, in GROMACS compatible format.

3 Results

3.1 Bond length and bond angle terms

The TPT force field parameters have been generated to be compatible with the *amber03* force field, and their reliability has been checked comparing the normal modes vibrational analysis calculated at B3LYP/6-31G* level with its counterpart at MM level. The results indicate an almost perfect correspondence between the two methods up to 1,400 cm^{-1}, while around 1,600 cm^{-1}, corresponding to the stretching of C–C, C–N, and C–O bonds, the agreement is somewhat less accurate (Fig. 2). QM and MM normal modes are again in good agreement for bonded interactions around 3,000 cm^{-1}, corresponding to stretching of the C–H bonds. For type 2a the MM parameter is less accurate around 2,400 cm^{-1} which corresponds to the stretching of the N–H bond. On the whole the results are in a very good agreement, being 0.9953 and 0.9965 the correlation between the two sets of data in the type 2a and 2b form, respectively. As a further validation, QM harmonic frequencies have been compared to the IR experimental band positions in the TPT–HCl pentahydrate crystal [41]

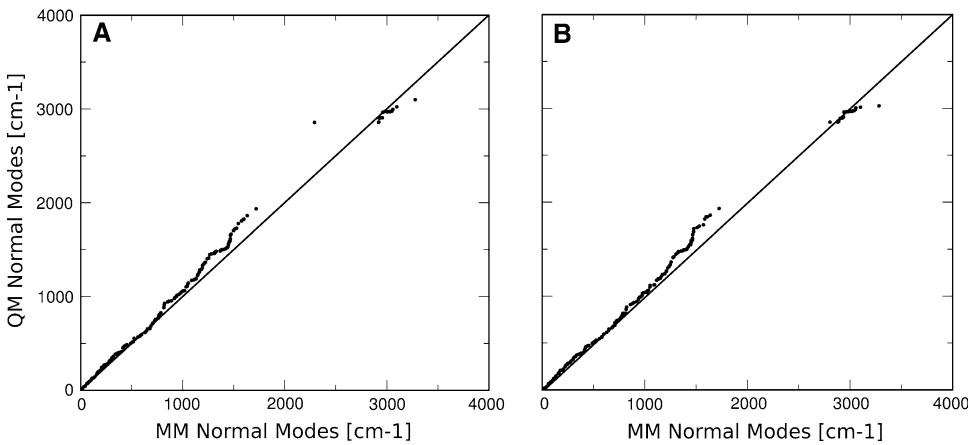

Fig. 2 Comparison of quantum and classical frequencies of type 2a (**a**) and 2b (**b**) forms of topotecan

Table 1 Comparison between QM frequencies (scaled by a factor of 0.9613) and IR frequencies of TPT–HCl pentahydrate crystals [41]

QM freq. (cm^{-1})	QM normal mode	IR freq. [41]	Assignment [41]
1,722	C=O lactone	1,754, 1,745, 1,740	C=O lactone
1,636	C=O amide	1,658	C=O amide
1,609	C=N aromatic	1,649	C=N aromatic
1,595	C=C ar., C=N ar.	1,596	C=C aromatic
1,582	C=C aromatic	1,584	C=C aromatic
1,569	C=C aromatic		
1,529	C=C aromatic		
1,508	C=C aromatic	1,506	C=C aromatic

Assignment of QM normal modes have been made by observation with Molden visualization software

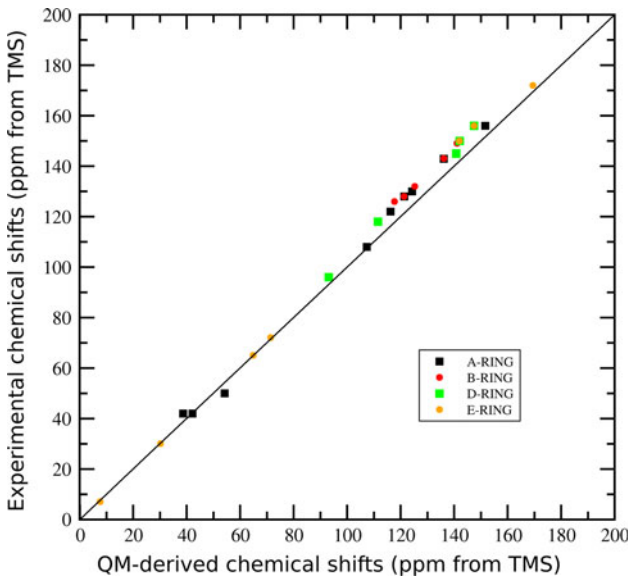

Fig. 3 Comparison between experimental ^{13}C and QM chemical shift derived from magnetic shielding calculated with the gauge independent atomic orbital method at the B3LYP/6-31G* level

(Table 1). The results are very satisfactory with the slight exception of the frequencies assigned to the stretching modes of the lactone and amide carbonylic bonds, which, however, result to be a hydrogen-bonding site in the TPT–HCl pentahydrate crystal. A third evaluation of the accuracy of our quantum mechanical description of TPT has been performed comparing experimental [41, 42] and QM-derived ^{13}C chemical shifts. The correlation between experimental and theoretical data, shown in Fig. 3, is 0.9988. These results confirm that that the overall performance of the B3LYP/6-31G* level of theory is adequate to describe the TPT electronic properties and that the *amber03* parameters can be directly used in the classical MD simulations of drug–enzyme–DNA complexes, applying the typical constrains to treat hydrogen atom dynamics [43].

3.2 Dimethylamino group of ring A

TPT differs from CPT by the two substitutions in positions 9 and 10 of ring A (Fig. 4). These modifications make TPT more soluble, and decrease its half life and toxicity, thus reducing the problem of drug accumulation at the increase of daily doses [44–46].

Particular attention, has been paid to the force field parametrization of these groups, to model the TPT–DNA and TPT–enzyme interactions. The conformational degree of freedom of the dimethylamino group in position 9 can be described by two dihedral angles (α and β in Fig. 4). The potential energy surface (PES) of this group has been characterized through calculation of the QM energy of several TPT conformations, obtained by systematically changing the values of the two dihedral angles. A reduced model of TPT, consisting of the A + B ring quinoline subunit of the molecule, has been used to build the PES. The resulting surfaces are shown in Fig. 5. The type 2a structure (panel A) has two potential energy minima (A_1 and A_2), symmetric with respect to the plane of ring A.

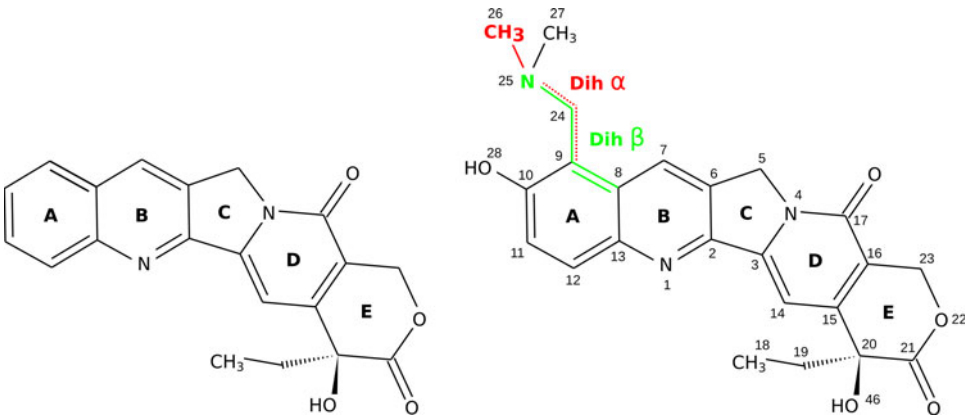

Fig. 4 Chemical structure of campthotecin (*left*) and topotecan (*right*). Principal dihedral angle of the dimethylamino substituent in position 9 are highlighted

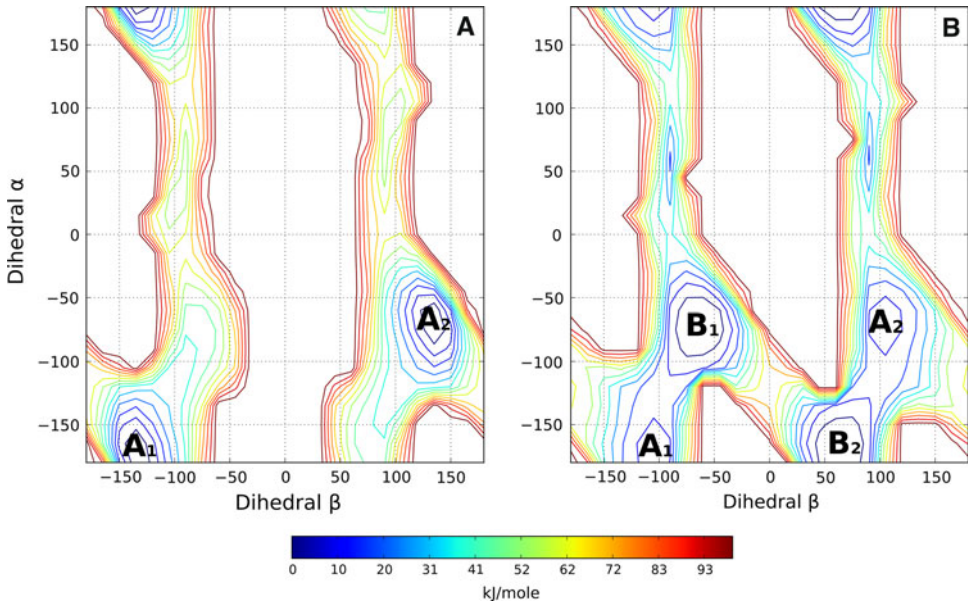

Fig. 5 PES of the two dihedral angles α and β describing the orientation of the dimethylamino group, calculated over a simplified model of topotecan, at B3LYP/6-31G* + PCM level of theory. *Panel A* type 2a tautomer showing the presence of a single minimum A_1 and its symmetric conformation A_2; *Panel B* type 2b tautomer showing the presence of two minima A_1 and B_1 and their symmetric conformations A_2 and B_2

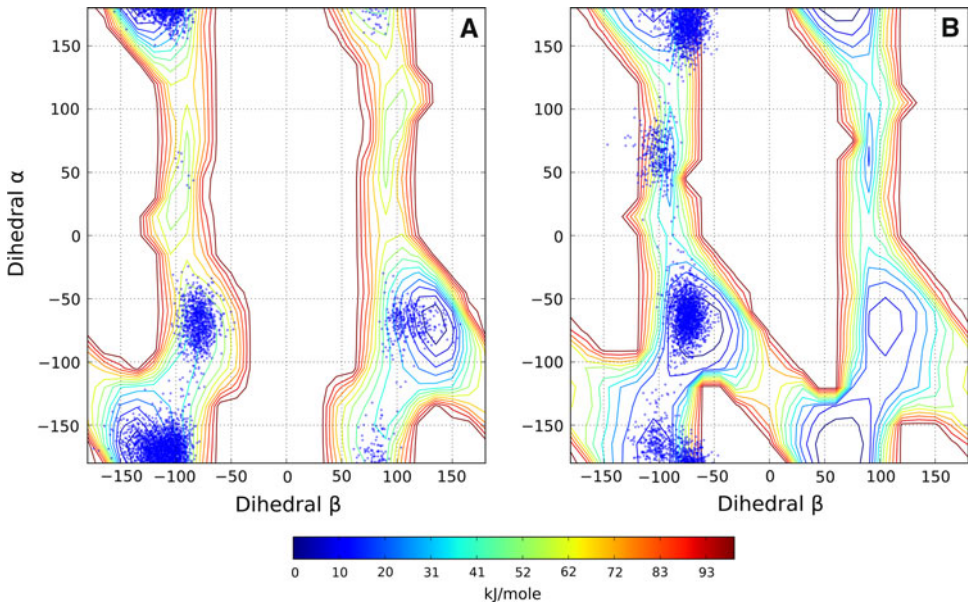

Fig. 6 Superimposition of PES of the two dihedral angles α and β with the values (*blue dots*) visited during the MD simulations performed using the RESP charges calculated on the global minimum for each conformation. *Panel A* type 2a trajectory; *Panel B* type 2b trajectory

On the other hand, the PES of type 2b (panel B) shows the presence of four minima, with the two indicated by A_2 and B_2 symmetric to A_1 and B_1 with respect to the plane of ring A.

To test the capability of the classical force field to reproduce the QM-level PES, we performed MD simulations of both type 2a and 2b TPT tautomers in water. Atomic charges were obtained by fitting the results of ab initio calculations applying the RESP method [27, 28]. To ensure sufficient sampling of conformational basins in the two systems, two 20 ns simulations were performed. This sampling time is very long as compared to expected relaxation rate for the rotation around α and β, and should assure a very accurate reproduction of the phase space. For instance, relaxation rates of most aminoacid side chains, even with much bulkier substitutes than a $-N(CH_3)_2$ group, are of the order of $10–10^2$ ps [47]. The time needed to move to one conformational basin to another can be

Table 2 Ab initio energy values for TPT type 2b geometry optimization at B3LYP/6-31G* + PCM level of theory are reported for the four minima shown in Fig. 4, together with the relative dihedral angle values

Dihedral angle α (°)	Dihedral angle β (°)	Energy (au)	Name in Fig. 4
−167,38	−103,03	−1430.725522	A_1
−61,73	−56,93	−1430.728025	B_1
−171,26	57,50	−1430.727890	B_2
−68,42	103,72	−1430.725314	A_2

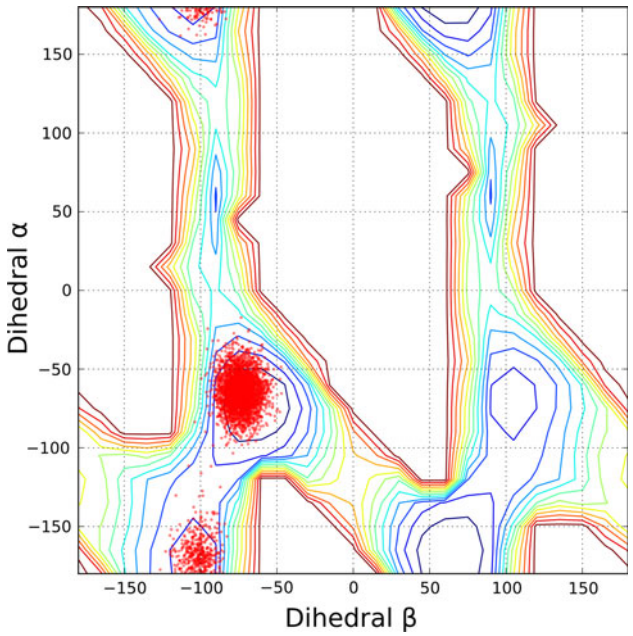

Fig. 7 Superimposition of PES of the two dihedral angles α and β of type 2b with the dihedral angle values (*red dots*) visited during the MD simulations using the MultiRESP charges

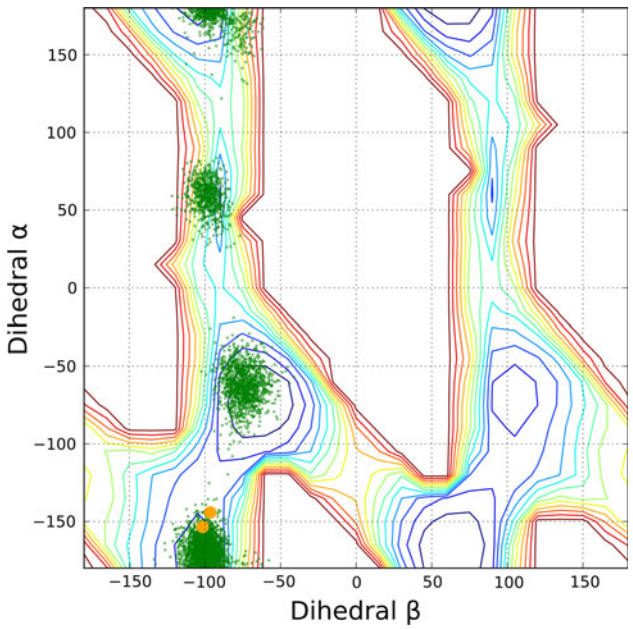

Fig. 8 Superimposition of PES of the two dihedral angles α and β of type 2b with the dihedral angle values (*green dots*) visited during the MD simulations of the Top1–DNA–TPT ternary complex, performed using the MultiRESP charges for the TPT molecule. Dihedral angle values of the two available TPT ternary complex crystal structures (PDB: 1K4T) are indicated with two *red circles*

estimated using the time decay constant τ of the dihedral autocorrelation function, since this quantity is strictly related to the mean residence time spent in each allowed

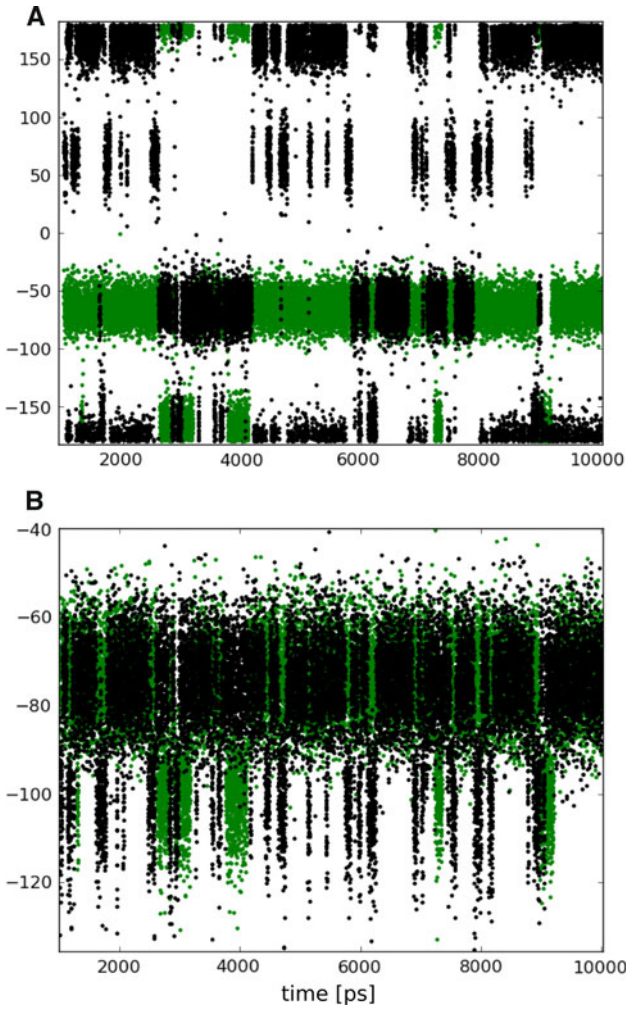

Fig. 9 Dihedral angles α and β values as a function of time calculated from the MultiRESP (*green dots*) and RESP (*black dots*) simulations of type 2a in water. *Panel A* values of the α dihedral angle. *Panel B* values of the β dihedral angle. The estimated relaxation time, calculated from dihedral auto-correlation of the MultiRESP trajectory, is 166 ps

conformation. Values of 9 and 127 ps are obtained for the α and β dihedral angles, respectively, in full agreement with results obtained for comparable systems. Visited conformations are shown in Fig. 6 as blue dots superimposed on the ab initio PESs.

The results in panel A show that the type 2a parametrization is very satisfactory since the α and β dihedral angle conformations visited during the simulation are close to the energy minima identified by the ab initio PES calculation. On the contrary, the results for type 2b are less satisfactory, since several configurations fall in PES regions characterized by high potential energy. The sampling of high conformational energy space regions observed in the type 2b trajectory can be explained by the assumption in the RESP procedure of the existence of a single potential energy minimum, but type 2b has two

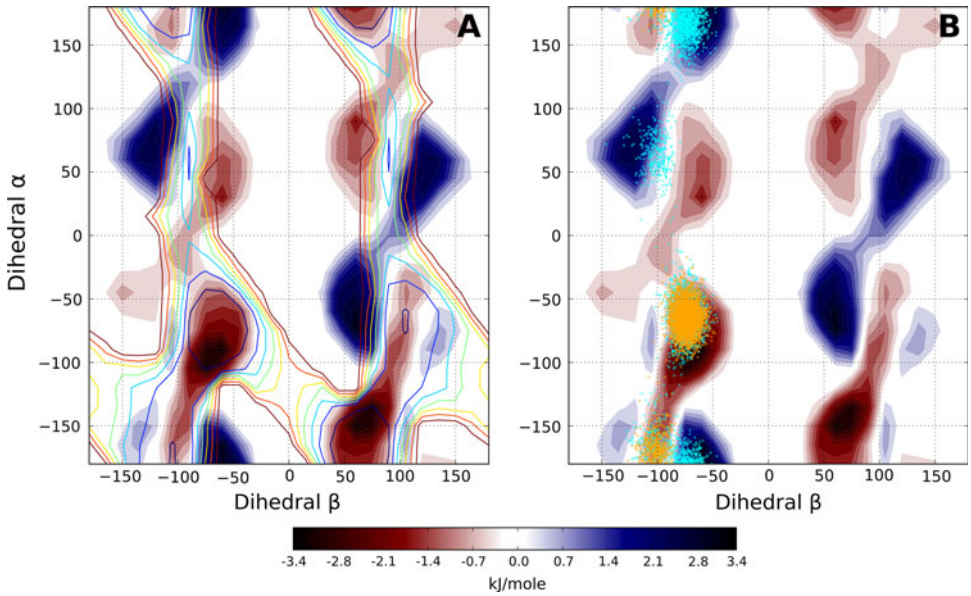

Fig. 10 **a** Superimposition of the FES difference, obtained from the metadynamic simulations, on the PES of the two dihedral angles α and β of type 2b. **b** Superimposition of the FES difference obtained from the metadynamic simulations with the point sampled during the MD simulations. *Cyan* and *orange* colors are used for configurations sampled using the RESP or MultiRESP charges, respectively

symmetric couples of energy minima (Fig. 5, panel B). In the case of multiple energy minima, the MultiRESP method [29] has been proven to yield better results. To this end, full ab initio geometry optimizations of the whole TPT molecule at the PCM(B3LYP/6-31G*) level have been carried out on the four minima conformations identified by the ab initio calculations and the relevant results are reported in Table 2. These new optimized molecular geometries were then used in the MultiRESP procedure of in Eq. 1, as reported in Sect. 2. Then, a new 20 ns MD simulation has been carried out using the MultiRESP atomic charges. The dihedral angle conformations visited during the new simulation are superimposed as red dots on the type 2b PES in Fig. 7. The two A_1–B_1 minima are now fully explored during the simulation and no high energy conformations were visited by the MD simulation. Therefore, the MultiRESP charges solve the electrostatic parametrization for the dimethylamino group of ring A in type 2b (compare panel B of Fig. 6 with Fig. 7).

It is worth noting that the parametrization of the dimethylamino group of ring A has a direct influence on the simulation of topoisomerase I–DNA interaction with the TPT anticancer drug. Preliminary MD results on the ternary topoisomerase I–DNA–TPT complex show, in fact, that the environment changes the probability to visit the A_1 or B_1 minima in the type 2b form, as shown by superimposing the dihedral angle conformations over the type 2b PES (green dots in Fig. 8). The results show a higher tendency of visiting the A_1 minimum region in the simulation of the ternary complex, while in water the B_1 minimum is preferred (compare red dots in Fig. 7 with green dots in Fig. 8). In line with these findings, the dihedral angle conformations in the two X-ray crystallographic structures of TPT in complex with Top1 and DNA [4] are in the A_1 minimum region (red circles in Fig. 8).

3.3 Comparison of MD results with non-equilibrium sampling approaches

As shown before, transition from one conformational minimum to another for the dimethylamino group is by no means a rare event in the simulated conditions, and several transitions between dihedral configurations are observed both in the MultiRESP and in the RESP simulations of type 2b (see Fig. 9). A quantitative evaluation of differences between the PES obtained using either the MultiRESP or RESP approaches can be obtained using a method aimed at reconstructing the multidimensional free energy of complex systems, such as metadynamics [35]. To this end, we performed two metadynamic simulations defining the α and β dihedral angles as collective variables (CVs) and using the two set of charges (MultiRESP or RESP) of TPT. Monitoring the evolution of CV during simulation we observed a progressive broadening of the fluctuations, related to the filling of free energy well. After 10 ns in both simulations the frequency of flipping of β dihedral angle between negative and positive values (that is the transition with the highest energy barrier, see Fig. 5b) becomes very high. To ensure a complete filling of energy wells we calculated the free energy surfaces (FES) summing 10^5 Gaussian hills corresponding to 20 ns of simulation.

Figure 10a shows the superposition of the QM-level potential energy surface (drawn as a contour plot) with the $\Delta\Delta G$ surface calculated as a difference of the FES: $\Delta\Delta G = \Delta G_{\text{MultiRESP}} - \Delta G_{\text{SimpleRESP}}$ (drawn using color code). Therefore, zones where the MultiRESP energy is lower

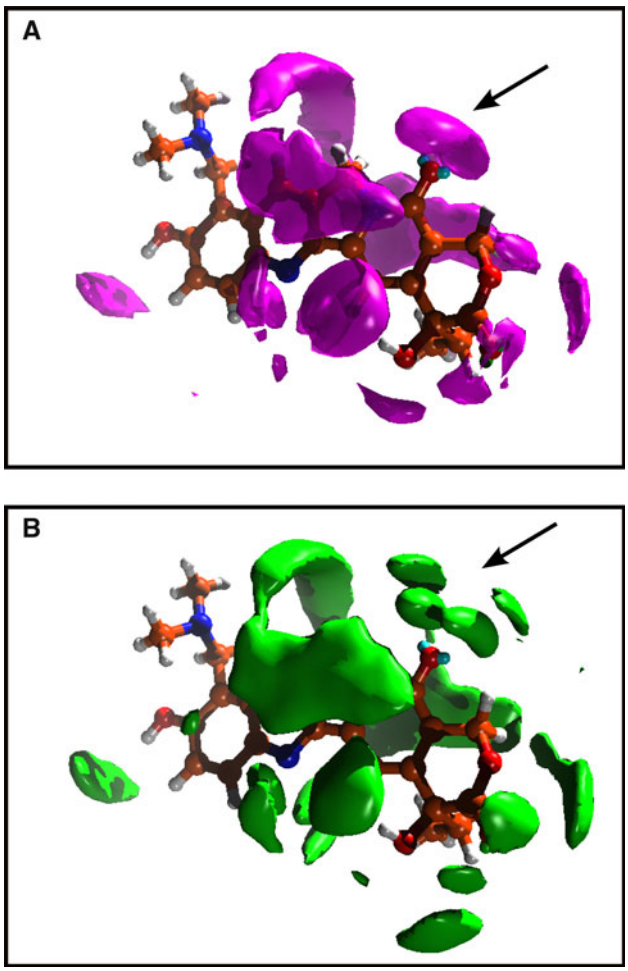

Fig. 11 **a** Comparison of the spatial distribution function (SDF) of water oxygen around TPT calculated over a MD simulation in explicit water solution on the carbonyl oxygen of rings D and E in absence of virtual sites. **b** The same, but in the presence of virtual sites. The *arrows* indicate the splitting of density observed in the presence of virtual sites, denoting the correct geometrical coordination of two water molecules

than the RESP one are shown in red, while a blue color is adopted when the MultiRESP energy is higher than the RESP one. The near-perfect coincidence of QM B1 minima with zones where the MultiRESP geometries are more stable is clearly visible. The difference of free energy in the B1 minimum is not very high $\Delta\Delta G = -3.44$ kJ/mole but, interestingly, an unfavorable blue region is visible at $\alpha \sim -160°$ and $\beta \sim -60°$. This corresponds to conformations sampled only in the RESP MD trajectory (see Fig. 6b) that are in a high-energy zone which should not be sampled at 300 K. In this case $\Delta\Delta G_{B_i} = +3.34$ kJ/mole Comparison of the $\Delta\Delta G$ surface obtained from the metadynamic simulations with the zones sampled by the simple MD trajectories (see Fig. 10b) shows that during the normal MD simulations the energy minima are explored very well using the MultiRESP or RESP charges and that simple MD trajectories are long enough to yield an accurate description of systems of this size complexity.

3.4 Ketone groups on rings D and E

Recently, we demonstrated that hydrogen bond interactions with the ketone group of CPT ring D modulate the wavelength of UV–Vis absorption bands of the drug, and that only by taking into account the electronic contribution of two interacting water molecules can all the experimental UV–Vis bands be reproduced [16]. This result indicates that an accurate modeling of the ketone groups on rings D and E is essential to reproduce precisely the drug interaction with the solvent or with the protein–DNA target. We have modeled these groups by adding two virtual sites on each oxygen atom and assigning half of the oxygen atomic charge to each virtual site, making the ketone oxygen atom neutral. These virtual sites allow a better hydrogen bonding directionality, mimicking the electronic localization of the two oxygen lone pairs. Such a procedure has already been used successfully for the MM parametrization of the acetone molecule allowing the reproduction of several UV and NMR spectroscopic properties [48]. The virtual sites constrain the spatial distribution of water hydrogen atoms around the TPT molecule as observed in Fig. 11, where the first shell water molecules near the carbonyl group on ring D form two distinct surfaces if virtual sites are used.

4 Conclusions

The anticancer drug topotecan in the lactonic form has been fully parametrized following a procedure compliant with the *amber03* force field parametrization [26], based on quantum mechanics calculations, including solvent effects by means of continuum models. The proposed TPT classic molecular mechanics force field is able to reproduce the internal flexibility of the molecule and the interaction with the solvent or the DNA–topoisomerase enzyme target. Adoption of this method allows the easy generation of force fields for other CPT derivatives and in principle even for the carboxylate forms. This work paves the route toward a structural and dynamic investigation on the role of this class of anticancer drugs in the inhibition of the topoisomerase enzyme and in the mechanism of resistance of topoisomerase mutants.

Acknowledgments The authors would like to thank C. Zazza for his contribution to data analysis and comments, and Prof. Jens Z. Pedersen for help in revising the manuscript. This work was partly supported by grants 'Characterization of human topoisomerase I mutants resistant to camptothecin and its derivatives' from AIRC (Associazione Italiana Ricerca Cancro) to A. D. and FILAS-Lazio

regional agency under the project CAMPTOFAR. We acknowledge CASPUR Supercomputing Consortium for computational resources.

References

1. Wall ME, Wani MC, Cook CE, Palmer KH, Mcphail AT, Sim GA (1966) Plant antitumor agents. I. The isolation and structure of camptothecin, a novel alkaloidal leukemia and tumor inhibitor from camptotheca acuminata. J Am Chem Soc 88:3888–3890
2. Pommier Y (2006) Topoisomerase I inhibitors: camptothecins and beyond. Nat Rev Cancer 6:789–802
3. Pommier Y, Pourquier P, Fan Y, Strumberg D (1998) Mechanism of action of eukaryotic DNA topoisomerase I and drugs targeted to the enzyme. Biochim Biophys Acta Gene Struct Expr 1400:83–105
4. Staker BL, Feese MD, Cushman M, Pommier Y, Zembower D, Stewart L, Burgin AB (2005) Structures of three classes of anticancer agents bound to the human topoisomerase I-DNA covalent complex. J Med Chem 48:2336–2345
5. Staker BL, Hjerrild K, Feese MD, Behnke CA, Burgin AB, Stewart L (2002) The mechanism of topoisomerase I poisoning by a camptothecin analog. Proc Natl Acad Sci USA 99:15387–15392
6. Chrencik JE, Staker BL, Burgin AB, Pourquier P, Pommier Y, Stewart L, Redinbo MR (2004) Mechanisms of camptothecin resistance by human topoisomerase I mutations. J Mol Biol 339:773–784
7. Fiorani P, Bruselles A, Falconi M, Chillemi G, Desideri A, Benedetti P (2003) Single mutation in the linker domain confers protein flexibility and camptothecin resistance to human topoisomerase I. J Biol Chem 278:43268–43275
8. Fiorani P, Chillemi G, Losasso C, Castelli S, Desideri A (2006) The different cleavage DNA sequence specificity explains the camptothecin resistance of the human topoisomerase I Glu418-Lys mutant. Nucleic Acids Res 34:5093–5100
9. Losasso C, Cretaio E, Fiorani P, D'Annessa I, Chillemi G, Benedetti P (2008) A single mutation in the 729 residue modulates human DNA topoisomerase IB DNA binding and drug resistance. Nucleic Acids Res 36:5635–5644
10. Chillemi G, D'Annessa I, Fiorani P, Losasso C, Benedetti P, Desideri A (2008) Thr729 in human topoisomerase I modulates anti-cancer drug resistance by altering protein domain communications as suggested by molecular dynamics simulations. Nucleic Acids Res 36:5645–5651
11. Fiorani P, Tesauro C, Mancini G, Chillemi G, D'Annessa I, Graziani G, Tentori L, Muzi A, Desideri A (2009) Evidence of the crucial role of the linker domain on the catalytic activity of human topoisomerase I by experimental and simulative characterization of the Lys681Ala mutant. Nucleic Acids Res 37:6849–6858
12. Chillemi G, Fiorani P, Castelli S, Bruselles A, Benedetti P, Desideri A (2005) Effect on DNA relaxation of the single Thr718Ala mutation in human topoisomerase I: a functional and molecular dynamics study. Nucleic Acids Res 33:3339–3350
13. Siu F-M, Che C-M (2008) Persistence of camptothecin analog–topoisomerase I–DNA ternary complexes: a molecular dynamics study. J Am Chem Soc 130:17928–17937
14. Bocian W, Kawcki R, Bednarek E, Sitkowski J, Williamson MP, Hansen PE, Kozerski L (2008) Binding of topotecan to a nicked DNA oligomer in solution. Chem Eur J 14:2788–2794
15. Sanna N, Chillemi G, Grandi A, Castelli S, Desideri A, Barone V (2005) New hints on the Ph-driven tautomeric equilibria of the topotecan anticancer drug in aqueous solutions from an integrated spectroscopic and quantum-mechanical approach. J Am Chem Soc 127:15429–15436
16. Sanna N, Chillemi G, Gontrani L, Grandi A, Mancini G, Castelli S, Zagotto G, Zazza C, Barone V, Desideri A (2009) UV–Vis spectra of the anticancer campothecin family drugs in aqueous solution: Specific spectroscopic signatures unraveled by a combined computational and experimental study. J Phys Chem B 113:5369–5375
17. Bailly C (2003) Homocamptothecins: potent topoisomerase I inhibitors and promising anticancer drugs. Crit Rev Oncol/Hematol 45:91–108
18. Frisch MJ, Trucks GW, Schlegel HB, Scuseria GE, Robb MA, Cheeseman JR, Montgomery JA, Vreven T, Kudin KN, Burant JC, Millam JM, Iyengar SS, Tomasi J, Barone V, Mennucci B, Cossi M, Scalmani G, Rega N, Petersson GA, Nakatsuji H, Hada M, Ehara M, Toyota K, Fukuda R, Hasegawa J, Ishida M, Nakajima T, Honda Y, Kitao O, Nakai H, Klene M, Li X, Knox JE, Hratchian HP, Cross JB, Bakken V, Adamo C, Jaramillo J, Gomperts R, Stratmann RE, Yazyev O, Austin AJ, Cammi R, Pomelli C, Ochterski JW, Ayala PY, Morokuma K, Voth GA, Salvador P, Dannenberg JJ, Zakrzewski VG, Dapprich S, Daniels AD, Strain MC, Farkas O, Malick DK, Rabuck AD, Raghavachari K, Foresman JB, Ortiz JV, Cui Q, Baboul AG, Clifford S, Cioslowski J, Stefanov BB, Liu G, Liashenko A, Piskorz P, Komaromi I, Martin RL, Fox DJ, Keith T, Laham Al MA, Peng CY, Nanayakkara A, Challacombe M, Gill PMW, Johnson B, Chen W, Wong MW, Gonzalez C, Pople JA (2004) Gaussian 03, Revision C.02. Gaussian, Inc., Wallingford, CT
19. Cossi M, Scalmani G, Rega N, Barone V (2002) New developments in the polarizable continuum model for quantum mechanical and classical calculations on molecules in solution. J Chem Phys 117:43–54
20. Rauhut G, Pulay P (1995) Transferable Scaling Factors for Density Functional Derived Vibrational Force Fields. J Phys Chem 99:3093–3100
21. Vemparala S, Ivanov I, Pophristic V, Spiegel K, Klein ML (2006) Ab initio calculations of intramolecular parameters for a class of arylamide polymers. J Comput Chem 27:693–700
22. Aleksandrov A, Simonson T (2009) Molecular mechanics models for tetracycline analogs. J Comput Chem 30:243–255
23. Mohandas P, Umapathy S (1997) Density-functional studies on the structure and vibrational spectra of transient intermediates of *p*-benzoquinone. J Phys Chem A 101:4449–4459
24. Wolinski K, Hinton JF, Pulay P (1990) Efficient implementation of the gauge-independent atomic orbital method for NMR chemical shift calculations. J Am Chem Soc 112:8251–8260
25. Jameson A, Jameson C (1987) Gas-phase 13C chemical shifts in the zero-pressure limit: refinements to the absolute shielding scale for 13C. Chem Phys Lett 134:461–466
26. Duan Y, Wu C, Chowdhury S, Lee MC, Xiong G, Zhang W, Yang R, Cieplak P, Luo R, Lee T, Caldwell J, Wang J, Kollman P (2003) A point-charge force field for molecular mechanics simulations of proteins based on condensed-phase quantum mechanical calculations. J Comput Chem 24:1999–2012
27. Bayly CI, Cieplak P, Cornell WD, Kollman PA (1993) A well-behaved electrostatic potential based method using charge restraints for deriving atomic charges: the RESP model. J Phys Chem 97:10269–10280
28. Cornell WD, Cieplak P, Bayly CI, Kollman PA (1993) Application of RESP charges to calculate conformational energies, hydrogen bond energies and free energies of solvation. J Am Chem Soc 115:9620–9631
29. Cieplak P, Cornell WD, Bayly C, Kollman PA (1995) Application of the multimolecule and multiconformational RESP methodology to biopolymers: charge derivation for DNA, RNA and proteins. J Comput Chem 16:1357–1377
30. Mobley, DL, Chodera JD, Dill KA (2006) On the use of orientational restraints and symmetry corrections in alchemical free energy calculations. J Chem Phys 125:084902+

31. Sorin EJ, Pande VS (2005) Empirical force-field assessment: the interplay between backbone torsions and noncovalent term scaling. J Comput Chem 26:682–690
32. Berendsen HJC, Postma JPM, van Gunsteren WF, Dinola A, Haak JR (1984) Molecular dynamics with coupling to an external bath. J Chem Phys 81:3684–3690
33. Darden T, York D, Pedersen L (1993) Particle mesh Ewald: an N [center-dot] log(N) method for Ewald sums in large systems. J Chem Phys 98:10089–10092
34. Hess B, Bekker H, Berendsen HJ, Fraaije C, Johannes GEM (1997) LINCS: a linear constraint solver for molecular simulations. J Comput Chem 18:1463–1472
35. Laio A, Parrinello M (2002) Escaping free-energy minima. Proc Natl Acad Sci USA 99:12562–12566
36. van der Spoel D, Berendsen HJ (1997) Molecular dynamics simulations of Leu-enkephalin in water and DMSO. Biophys J 72:2032–2041
37. Pettersen EF, Goddard TD, Huang CC, Couch GS, Greenblatt DM, Meng EC, Ferrin TE (2004) UCSF chimera—a visualization system for exploratory research and analysis. J Comput Chem 25:1605–1612
38. Grace. http://plasma-gate.weizmann.ac.il/Grace/
39. Octave. http://www.gnu.org/software/octave/index.html
40. Hunter J, Matplotlib. http://matplotlib.sourceforge.net/users/credits.html
41. Vogt F, Dellorco P, Diederich A, Su Q, Wood J, Zuber G, Katrincic L, Mueller R, Busby D, Debrosse C (2006) A study of variable hydration states in topotecan hydrochloride. J Pharm Biomed Anal 40:1080–1088
42. Zhao H, Lee C, Sai P, Choe YH, Boro M, Pendri A, Guan S, Greenwald RB (2000) 20-*O*-acylcamptothecin derivatives: evidence for lactone stabilization. J Org Chem 65:4601–4606
43. Stocker U, Juchli D, van Gunsteren WF (2003) Increasing the time step and efficiency of molecular dynamics simulations: optimal solutions for equilibrium simulations or structure refinement of large biomolecules. Mol Simul 29:123–138
44. Verweij J, Lund B, Beijnen J, Planting A, de Boer-Dennert M, Koier I, Rosing H, Hansen H (1993) Phase I and pharmacokinetics study of topotecan, a new topoisomerase I inhibitor. Ann Oncol: Official Journal of Eur Soc Med Oncol/ESMO 4:673–678
45. Burke TG, Mi Z (1994) The structural basis of camptothecin interactions with human serum albumin: impact on drug stability. J Med Chem 37:40–46
46. Rothenberg ML (1997) Topoisomerase I inhibitors: review and update. Ann Oncol: Official Journal of Eur Soc Med Oncol/ESMO 8:837–855
47. Kuczera K, Unruh J, Johnson CK, Jas GS (2009) Reorientations of aromatic amino acids and their side chain models: anisotropy measurements and molecular dynamics simulations. J Phys Chem A (in press). doi:10.1021/jp907382h
48. Pavone M, Brancato G, Morelli G, Barone V (2006) Spectroscopic properties in the liquid phase: combining high-level ab initio calculations and classical molecular dynamics. ChemPhysChem 7:148–156